Atmos. Meas. Tech. Discuss., 8, 4413–4449, 2015
www.atmos-meas-tech-discuss.net/8/4413/2015/
doi:10.5194/amtd-8-4413-2015

Atmospheric Measurement Techniques Discussions
Open Access

APOLLO_NG – a probabilistic interpretation of the APOLLO legacy for AVHRR heritage channels

L. Klüser, N. Killius, and G. Gesell

German Aerospace Center, German Remote Sensing Datacenter, Oberpfaffenhofen, Wessling, Germany

Received: 19 March 2015 – Accepted: 30 March 2015 – Published: 30 April 2015

Correspondence to: L. Klüser (lars.klueser@dlr.de)

Published by Copernicus Publications on behalf of the European Geosciences Union.

Abstract

The cloud processing scheme APOLLO (Avhrr Processing scheme Over cLouds, Land and Ocean) has been in use for cloud detection and cloud property retrieval since the late 1980s. The physics of the APOLLO scheme still build the backbone of a range of cloud detection algorithms for AVHRR (Advanced Very High Resolution Radiometer) heritage instruments. The APOLLO_NG (APOLLO_NextGeneration) cloud processing scheme is a probabilistic interpretation of the original APOLLO method. While building upon the physical principles having served well in the original APOLLO a couple of additional variables have been introduced in APOLLO_NG. Cloud detection is not performed as a binary yes/no decision based on these physical principals but is expressed as cloud probability for each satellite pixel. Consequently the outcome of the algorithm can be tuned from clear confident to cloud confident depending on the purpose. The probabilistic approach allows to retrieving not only the cloud properties (optical depth, effective radius, cloud top temperature and cloud water path) but also their uncertainties. APOLLO_NG is designed as a standalone cloud retrieval method robust enough for operational near-realtime use and for the application with large amounts of historical satellite data. Thus the radiative transfer solution is approximated by the same two stream approach which also had been used for the original APOLLO. This allows the algorithm to be robust enough for being applied to a wide range of sensors without the necessity of sensor-specific tuning. Moreover it allows for online calculation of the radiative transfer (i.e. within the retrieval algorithm) giving rise to a detailed probabilistic treatment of cloud variables. This study presents the algorithm for cloud detection and cloud property retrieval together with the physical principles from the APOLLO legacy it is based on. Furthermore a couple of example results from on NOAA-18 are presented.

1 Introduction

The cloud analysis tool APOLLO (Avhrr Processing Over cLouds, Land and Ocean) has been in use at DLR for more than 25 years now. It has been developed for cloud detection from Advanced Very High Resolution Radiometer (AVHRR) observations (Saunders and Kriebel, 1988) and has been expanded (e.g. Gesell et al., 1989) and updated (Kriebel et al., 2003) on several occasions. The AVHRR cloud detection with APOLLO also has been evaluated a couple of times (Kriebel et al., 2003; Meerkötter et al., 2004). Also in a wide range of other applications APOLLO has been used in adaptations to different satellite sensors. With observations of the (Advanced) Along-Track Scanning Radiometer ((A)ATSR) it has been used as cloud screening method for aerosol retrievals (Holzer-Popp et al., 2002) and with Spinning Enhanced Visible and InfraRed Imager (SEVIRI) observations for cloud screening as input to an infrared desert dust index (Klüser and Schepanski, 2009). Especially for the use with AATSR it also has undergone another sensor-specific update round dedicated to the needs of cloud screening for aerosol retrieval purposes (Holzer-Popp et al., 2008). It has been used in dedicated experiments within the aerosol project (Aerosol_cci) of the Climate Change Initiative (CCI) of the European Space Agency (ESA). Moreover APOLLO input has been used to address solar radiation issues (Schroedter-Homscheidt et al., 2013). It has furthermore been attempted to investigate the impact of desert dust aerosol on cloud properties from APOLLO data and collocated aerosol retrievals (Klüser and Holzer-Popp, 2010).

During all these years of research with use of APOLLO a couple of limitations have been identified (e.g. Klüser and Holzer-Popp, 2010) and different versions of the algorithms evolved (e.g. Kriebel et al., 2003; Holzer-Popp et al., 2008; Klüser and Schepanski, 2009; Klüser and Holzer-Popp, 2010), which made it desirable to initiate another major update of the method and to harmonise the sensor dependent versions again. Besides obviously necessary updates like the introduction of a cloud droplet effective radius retrieval along the optical depth estimation (Nakajima and King, 1990) and

AMTD
8, 4413–4449, 2015

the use of modern representations of ice cloud optical properties (Baum et al., 2014) especially the analyses conducted within the CCI experiments indicated the need for rethinking the cloud detection approach (Holzer-Popp et al., 2013).

As a direct consequence a new probabilistic cloud detection scheme has been developed from the basis of the APOLLO physics. One major goal of the next generation method is to be applicable with any satellite sensor, as long as the instrument provides the traditional five AVHRR channels (six as the change from 3.9 to 1.6 µm is incorporated), consequently also the new scheme does not use additional channels (like those centered at 8.7 µm or 13.4 µm) which are available on instruments such as SEVIRI or the new Visible Infrared Imaging Radiometer Suite (VIIRS) onboard the recently launched Suomi satellite. The probabilistic scheme still relies on the same physical assumptions, tests and metrics as the original APOLLO scheme. The scheme is specifically designed to be applied to the full AVHRR series, which lacks the information of such additional channels. Consequently we feel it is justified to still call the method APOLLO; but, as mathematically there has been a major step forward, the scheme will be called APOLLO_NextGeneration (or APOLLO_NG throughout this article). Moreover the AVHRR channel terminology is used, i.e. channel numbering from 1 to 5 with channel 1 referring to a red channel centered at 0.6 µm and channel 5 referring to an IR channel centered at 12 µm (see Kriebel et al., 2003).

Section 2 introduces the APOLLO_NG cloud detection algorithm based on APOLLO heritage and probabilistic principles. Section 3 deals with the detection of snow and its discrimination from clouds while Sect. 4 describes the retrieval of physical cloud properties subsequent to the cloud detection. It is followed by some examples in Sect. 5, a discussion of the algorithms and corresponding results in Sect. 6 and a concluding summary in Sect. 7.

AMTD
8, 4413–4449, 2015

2 Probabilistic cloud detection

2.1 Algorithm heritage

The original APOLLO cloud detection is based on five consecutive threshold tests, for which the thresholds are determined dynamically from the analyzed scene. Two of these tests are run twice with updated information. The succession of the respective tests feeds into a bit-adding scheme giving different weights to the different tests. Any observed AVHRR pixel is said to be cloud-contaminated or fully cloudy, if a sufficiently large number of bits are added (see Saunders and Kriebel, 1988; Kriebel et al., 2003).

The new APOLLO_NG cloud detection scheme is based on the same physical principles and thus channels respective channel combinations. But, instead of binary yes/no information gained from "simple" threshold tests, the distance from the respective threshold is used as an estimate of the likelihood of cloud presence in the observation. A Bayesian probability update scheme then uses the cloud probability (interpreted as confidence in observing a cloud) from the respective cloud test for updating the overall cloud probability. Although it seems not to be straightforward at first to interpret the distance of the observation from some threshold as a probability, it can be argued that a binary threshold testing scheme does exactly the same (see Fig. 1). Threshold methods assume, if an observed value is greater (respective lower) than that threshold, it is "definitely" cloudy or cloud free (depending on the threshold and the physical rationale). Thus it assigns a cloud probability of either 0 or 1 without allowing for fractional probabilities. That element then is introduced by weighting the binary 0/1 information in bit-adding schemes (see e.g. Kriebel et al., 2003 for details). Consequently the probabilistic extension just uses a mathematical treatment which on the one side is more flexible (allowing all probabilities between 0 and 1) and on the other hand stricter in the mathematical interpretation (propagating the determined probability in a clearly prescribed statistical way to the final cloud probability instead of assigning different weights to binary information).

AMTD
8, 4413–4449, 2015

After having obtained an estimate of the cloud probability, the cloud affected pixels (over land) undergo a snow detection test in the legacy of the Gesell et al. (1989) method. As before, instead of performing binary snow detection (yes/no decision), a snow probability is calculated which is based on a Bayesian treatment of different threshold-distance based snow presence estimators.

At night, only three infrared channels can be used due to the lack of sunlight and thus reflected radiation in the shortwave channels (Saunders and Kriebel, 1988; Kriebel et al., 2003). Consequently a different probabilistic cloud detection scheme is used for conditions without solar illumination.

The minimum value of cloud probability P_{cld} for assigning an observation to the cloud mask can be set differently. Thus the APOLLO_NG cloud detection can be tuned from clear sky confident (i.e. having low clear sky misclassification rate) to cloud confident (low cloud misclassification rate) as can be seen from Fig. 1.

Figure 2 shows the flowchart of the APOLLO_NG cloud detection and the decision tree for cloud property retrieval. The major contrast to the traditional APOLLO scheme is that the different cloud tests are stored as individual information and then are propagated to the total cloud probability instead of using a consecutive bit-adding method for cloud detection.

2.2 Cloud probability, Bayesian probability propagation and probabilistic information content

Probabilistic cloud detection aims at evaluating the probability of cloud occurrence in a given observation x. Observations in this sense can be any observed property like one-channel reflectance or brightness temperature, brightness temperature difference or reflectance ratios (see for example Kriebel et al., 2003; or Frey et al., 2008, for overviews of observations used for cloud detection). For any observation an interval between values with a very high confidence for representing cloud free background conditions (x_{bg}) and values with a very high confidence for representing cloud observations (x_{cld}) is defined. Figure 1 shows a schematic plot of the confidence interval

AMTD
8, 4413–4449, 2015

concept. x_{bg} and x_{cld} can be either predefined, potentially depending on some other observation y, or they are determined from the satellite observations themselves, e.g. by averaging over larger observation windows. The cloud probability for each cloud test then follows the linear metric

$$P_{test} = \frac{x - x_{bg}}{x_{cld} - x_{bg}}. \tag{1}$$

It can be assumed that any observation can be approximated by piecewise linearization around a traditional cloud mask threshold x_{binary} (which represents a confidence level of 0.5 in probabilistic terms). Thus x_{cld} and x_{bg} must be selected to meet this assumption realistically, i.e. the interval $[x_{bg}, x_{cld}]$ must not be too large for the character of given observation x.

Bayesian statistics is used to propagate cloud likelihood information within different tests to aggregate the information gained from the different inputs, but it is not used for propagating cloud likelihood between tests as they are sensitive to very different cloud types.

Generally the theorem of Bayes states that the likelihood of one event can be calculated from the likelihood of all possible events and is traditionally used for updating probability information for very different purposes (e.g. Rodgers, 1998; MacKay, 2003).

The version of Bayes theorem most often used in retrieval theory is

$$P(x|y) = \frac{P(y|x) \cdot P(x)}{P(y)} \tag{2}$$

where $P(x)$ is the a priori probability of the information to be retrieved, $P(y)$ is the evidence of the information from the observation, $P(y|x)$ is the likelihood of observation y given the value of x and $P(x|y)$ is the desired probability of the value for x given the evidence $P(y)$.

In the framework of cloud detection, one can assume that the evidence carrying signal is a binary symmetric channel, i.e. $P(\neg y) = 1 - P(y)$. This assumption becomes important when updating a probability. In this case, furthermore using $P(y) =$

Discussion Paper | Discussion Paper | Discussion Paper | Discussion Paper

AMTD

8, 4413–4449, 2015

APOLLO_NG – a probabilistic interpretation of the APOLLO legacy

L. Klüser et al.

Title Page
Abstract Introduction
Conclusions References
Tables Figures
Back Close
Full Screen / Esc
Printer-friendly Version
Interactive Discussion

$P(y|x)P(x) + P(y|\neg x)P(\neg x)$, the updated probability of x under the new evidence y becomes (MacKay, 2004)

$$P(x|y) = \frac{P(x) \cdot P(y|x)}{(1 - P(x)) \cdot (1 - P(y|x)) + P(x) \cdot P(y|x)} \tag{3}$$

which is more convenient for the purpose of cloud detection than Eq. (2).

As the information in all above described cloud tests is complementary, Eq. (3) is used for probability propagation if the respective likelihood $P(y|x)$ given by a cloud test is non-zero (i.e. $P(y|x) > 0$). If $P(y|x) = 0$, $P(x|y)$ remains unaffected by $P(y|x)$ as otherwise $P(x|y)$ would be zero as soon as one single test fails to detect the cloud. This would severely violate the physical concepts behind the original formulation of the APOLLO scheme.

The thus determined P_{cld} [$= P(x|y)$] describes the aggregated probability that an observation is cloud contaminated. It is obtained by consecutive likelihood updates described. Consequently it can be used for cloud masking based on the desired confidence in either clear sky or cloudy pixel detection (see also discussion in Holzer-Popp et al., 2013). It has to be clearly pointed out that $P_{cld} > 0$ does not intuitively tell anything about cloud properties.

In order to learn about the reliability of the cloud detection the cloud probabilities (those of the five different cloud tests outlined above) can be used as input to an assessment of Shannon's information content H_{inf} (Shannon and Weaver, 1949; Kolmogorov, 1968; Rodgers, 2000; MacKay, 2004). Therefore the probabilities for cloud observation have to be interpreted as independent signals (messages in the words of Shannon and Weaver, 1949). Five signals about the cloud state build the basis for the information content: P_{IGT}, P_{SCT}, P_{DVT}, P_{R21}, P_{T45}. In Shannon and Weaver (1949) the mathematical formulation of the information content requires that none of the probabilities equals 0 and also none equals one. Consequently every $P_x = 0$ would be set to 0.01 and every $P_x = 1$ would be set to 0.99 for the purpose of calculating Hinf.

AMTD
8, 4413–4449, 2015

APOLLO_NG – a probabilistic interpretation of the APOLLO legacy

L. Klüser et al.

Shannon and Weaver (1949) moreover outline, that it is required that the pieces of information (what they call "messages") form a set of probabilities, (i.e. with their sum being equal to 1), requiring normalization of the initially obtained cloud test probabilities. The information content of the cloud detection algorithm then simply is

$$H_{\mathrm{inf}} = -\sum_{j=1}^{5} P_j \cdot \log_2(P_j) \quad (4)$$

The probabilistic information content concept of Kolmogorov (1968) expands the view of Shannon and Weaver (1949) with respect to of Bayesian probability theory. Assuming that a priori information (i.e. information independent of the aforementioned cloud tests) is zero, Eq. (4) emerges from the considerations of Kolmogorov (1968) without the necessity of normalizing the cloud probabilities P_j. This is used as definition of cloud information content H_{inf} throughout this article.

It is intuitive from the very name of H_{inf}, that the magnitude of H_{inf} is related to the information carried by the vector of cloud probabilities. In the case of cloud detection the word information can be interpreted in the most obvious way: high information content signifies that the different probabilistic cloud tests agree quite well. This is a direct consequence of the definition of information content. Assume that the probabilities would highly disagree. Then including one of the tests with rather low probability thus would not add any new information to the knowledge about the cloudiness. In the sense of Shannon and Weaver (1949) all information about the cloud contamination would already be known by having the information of one or two tests. On the other hand, having similar probabilities in all tests each of it adds very valuable information in the meaning of additional knowledge. Thus the resulting high information content indicates that all cloud tests contribute to the knowledge about the cloud presence and the confidence increases that the pixel is really cloud contaminated. Consequently, high H_{inf} relates to a more homogenous distribution of the probabilities while low H_{inf} indicates the significance of merely a single test for cloud detection. The more tests indicate cloudy (or cloud free) conditions, the higher the confidence in the cloud detection. On the other

AMTD
8, 4413–4449, 2015

hand the original APOLLO was built in such a way that a single cloud test was able to classify an observation as cloudy. Consequently H_{inf} can be used as a quick reference to the quality, i.e. reliability, of the cloud detection. Together with P_{cld} it thus may be used to tune the output towards a more "clear confident" cloud mask or a more "cloud confident" cloud mask, depending on the purpose of the product.

2.3 Probabilistic cloud detection tests

2.3.1 Infrared Gross Temperature (IGT)

Thick or cold-topped clouds can easily be detected in infrared satellite imagery by their low brightness temperatures (e.g. Shenk and Curran, 1974; Rosenfeld and Lensky, 1998; Frey et al., 2008). The Infrared Gross temperature test (IGT) of the original APOLLO makes use of the deviation between observed cloudy brightness temperature in one of the split window channels and the background temperature representing the surface. In order to evaluate the brightness temperature distance from the most likely cloud contaminated brightness temperature, a 67 × 67 (±32 pixels) pixels box around the respective observations is evaluated. Kriebel et al. (2003) argue that over ocean surfaces a reflectance ratio for the channels 1 and 2 (centered at 0.6 and 0.9 µm respectively, slightly depending on the sensor) which is lower than 0.7 indicates mainly cloud free conditions.

Frey et al. (2008) use channel 2 reflectance to identify cloud free pixels with different confidence levels (see different thresholds over ocean, non-arid land and semi-arid or arid land in Frey et al., 2008, Table 2).

The channel 2 reflectance thresholds of Frey et al. (2008) with high confidence are used to filter all brightness temperatures in channel 5 (T_5, centered around 12 µm) in the 67 × 67 pixel window and to determine the average brightness temperature of these most likely cloud-free data. Given the case no sufficiently dark pixels are found over ocean, then the respective reflectance ratio threshold is used and only pixels with

AMTD
8, 4413–4449, 2015

smaller values then a high confidence threshold (Table 2 in Frey et al., 2008) are taken into account (this is identical to the approach of Kriebel et al., 2003).

If the 67 × 67 pixel window does not yield a valid background brightness temperature T_{bg}, e.g. due to an insufficient number of pixels passing the reflectance ratio filter, the window is expanded to a size of 257 × 257 pixels. Also the average brightness temperature threshold for cloud likelihood estimation (T_{min}) of the running window is estimated likewise with setting a channel 2 reflectance bound sufficiently high for approximating T_{min} by the maximum temperature of these supposedly cloudy pixels. That means in fact that each observation having channel 5 temperature colder than T_{min} is assumed to be cloud.

The aforementioned approach can be understood as clustering the data into confident cloud free and supposedly cloudy data and subsequent cluster-averaging. In order to speed up the procedure, T_{bg} and T_{min} are only calculated for 1 in 8 pixels and linearly interpolated in between (assuming steady and slowly varying background and cloud field temperature conditions, see e.g. Kriebel et al., 2003)

$$P_{IGT} = \frac{T_{bg} - T_5}{T_{bg} - T_{min}} \tag{5}$$

If $T_5 \leq 233.15$ K and $T_{bg} \leq 233.15$ K (homogeneous freezing threshold, Pavolonis and Heidinger, 2004) it can be assumed that the target is a synoptic scale convective system, when also $R_1 \geq 0.4$. Then P_{IGT} is set to 0.95 without evaluating eq. (%) as in large scale synoptic systems it may be extremely difficult to find the appropriate background temperature T_{bg}.

2.3.2 Spatial Coherence Test (SCT)

Clouds typically deviate from surface observations by being brighter and colder (e.g. Shenk and Curran, 1974; Rosenfeld and Lensky, 1998). The original spatial coherence test was used to examine regions with high variability in either reflectance or brightness

AMTD
8, 4413–4449, 2015

temperature (see Kriebel et al., 2003). In the APOLLO_NG algorithm the spatial coherence is evaluated consecutively in temperature and reflectance data at day and only in temperature data at night. It starts with evaluating the 3 × 3 pixel SD of the brightness temperature field (σ_{T_5}) and of the channel 2 reflectance field (σ_{R_2}). Of course the above explained approach can only be followed if the whole running window is either ocean or land, i.e. coastal pixels are discarded in the SCT likelihood. Moreover over land it is only applied when $P_{\mathrm{IGT}} > 0$.

Applying Eq. (3) the respective SCT cloud probability PSCT is then evaluated as

$$P_{\mathrm{SCT}} = \frac{\sigma_{T_5} \cdot \sigma_{R_2}}{(0.2 \cdot [1 - \sigma_{T_5}] \cdot [1 - \sigma_{R_2}/0.2] + \sigma_{T_5} \cdot \sigma_{R_2})} \tag{6}$$

with cloud likelihood normalization parameters of 1.0 K respective 0.2 for the SD of T_5 and R_2 (adapted from Kriebel et al., 2003). Physically that means, the higher the SD (the more variable the reflectance respective temperature field), the higher is the likelihood that the window is cloud affected and is mostly sensitive to broken or inhomogeneous cloud fields within the observation window.

2.3.3 Dynamic Visible Test (DVT)

Clouds can be identified as bright reflecting objects in satellite images (e.g. Shenk and Curran, 1974) Many different approaches have been identified to use reflectance thresholds for cloud discrimination (examples listed in e.g. Nakajima and Kaufman, 1993; Frey et al., 2008; Klüser et al., 2008). The dynamic visible daytime scheme in the original APOLLO uses dynamic thresholds based on channel 2 (over ocean) or channel 1 (over land) reflectance histograms for cloud identification. The approach is analogous to the IGT approach, but the scaling is performed with minimum cloudy and maximum clear sky reflectance for given confidence levels (again from Frey et al., 2008) of the moving window instead of minimum brightness temperature. Consequently the

DVT cloud likelihood is formulated as

$$P_{\mathrm{DVT}} = \frac{R_{1,2} - R_{\mathrm{bg}}}{R_{\mathrm{bg}} - R_{\mathrm{max}}} \tag{7}$$

and R_{bg} and R_{max} are again evaluated for land and ocean separately. Applying only Eq. (7) with the cluster-based background and maximum reflectance values would result in high cloud probabilities over various land surfaces such as deserts or other bright surfaces. Thus the cloud probability is updated with Eq. (3) by using a priori background values for arid and non-arid land surfaces depending on the observed scenery. Following Frey et al. (2008) land surfaces are distinguished between arid and non-arid (i.e. vegetated) by the minimum channel 1 reflectance in the running window. If the minimum reflectance falls below the clear sky value (high confidence) for non-arid land or the brightness temperature of the background is lower than 285 K, the filtering uses the non-arid values and the arid boundary thresholds are used otherwise. Any residual misinterpretation of desert surface properties for cloud probability is excluded by flagging all pixels having nonnegative P_{DVT}, being warmer than 278 K, darker than 0.6 and having negative split window brightness temperature difference of $T_4 - T_5$ (see e.g. Klüser and Schepanski, 2009, on the use of brightness temperature difference over deserts). Also very warm pixels ($T_5 > 290$ K) for which the reflectance ratio test (see 2.6) yields zero probability are discarded over land (see also discussion on warm top clouds in Holzer-Popp et al., 2008). For these desert pixels P_{DVT} is set back to 0.

Over water bodies the DVT test is also sensitive to sunglint, i.e. direct reflection of sunlight at the water surface. In former versions of APOLLO the DVT has not been applied within the area potentially affected by sunglint, which can be determined from theoretical considerations (Saunders and Kriebel, 1988). The test, if a pixel is sunglint or not, can also be evaluated from the observations and feeding back into the DVT cloud probability. Once an observation is within the sunglint area and IGT and SCT do not indicate high cloud likelihood (i.e. $P_{\mathrm{IGT}} < 0.5$ and $P_{\mathrm{SCT}} < 0.5$) the DVT probability is assumed to merely represent sunglint, if the magnitude of the deviation of T_2 from the 3×3 pixel mean exceeds 0.125 K (Kriebel et al., 2003).

2.3.4 Shortwave reflectance ratio (R21)

Due to the typical optical properties of clouds as well as land and water surfaces, the ratio of shortwave reflectance (i.e. between the AVHRR channels 2 and 1 centered around 0.9 and 0.6 µm respectively) provides information about the likelihood of clouds compared to open water bodies or land surfaces (see also the filtering in the IGT thresholds). Clouds usually occupy reflectance ratios between 0.7 and 1.3 (Kriebel et al., 2003). The peak of the reflectance ratio histogram in the moving window is determined according to the description by Saunders and Kriebel (1988). The distance of the actual observation from the peak is used to calculate P_{R21}, if it is smaller than 0.2 (widens the original threshold of Saunders and Kriebel (1988), in order to allow for a wider range of probabilities):

$$P_{\mathrm{R21}} = \frac{|(R_2/R_1) - (R_2/R_1)_{\mathrm{peak}}|}{0.2} \tag{8}$$

In contrast to Kriebel et al. (2003) the reflectance ratio is used for cloud probability not only over water bodies, but also over land (requiring that $T_5 < 285$ and $T_4 - T_5 > 0$ in order to exclude warm desert surfaces). If the conditions for potential sunglint are met (see above), R_{21} is interpreted as contribution to the sunglint probability instead of using it for determining cloud probability (in perfect analogy to the approach for DVT).

2.3.5 Brightness temperature difference (T45)

The test for thin clouds and cirrus is one of the most important for a couple of applications (e.g. Holzer-Popp et al., 2013). Thin clouds can be detected by their differential influence on brightness temperatures at 11 and 12 µm (the so called split window channels) due to slopes in the complex refractive index of water and ice in that spec-

AMTD
8, 4413–4449, 2015

tral region (e.g. Warren, 1984). Especially for cirrus clouds the extinction efficiency is much lower at 11 than at 12 µm (Yang et al., 2005). The Brightness Temperature Difference (BTD) of AVHRR channels 4 and 5 is used frequently for cirrus detection and visualization (e.g. Rosenfeld and Lenksy, 1998; Frey et al., 2008).

The thresholds for thin cloud detection vary with observed channel 4 brightness temperature as well as with the cosine of the viewing zenith angle Θ_v (Saunders and Kriebel, 1988). In order to determine the cirrus probability from the T45 test as outlined in Kriebel et al. (2003) the BTD thresholds are evaluated for a range of conditions enveloping the actual conditions (namely, T_4 and $\cos(\Theta v)$). From these envelope conditions the minimum and maximum BTD (named $\mathrm{BTD_{min}}$ and $\mathrm{BTD_{max}}$, respectively) are determined and the thin cloud probability is evaluated as for the other tests:

$$P_{\mathrm{T45}} = \frac{\mathrm{BTD} - \mathrm{BTD_{min}}}{\mathrm{BTD_{max}} - \mathrm{BTD_{min}}} \tag{9}$$

2.3.6 Additional nighttime probability estimates (T43 and T35)

At night the channels 1 and 2 cannot be exploited for cloud detection, as no reflected sunlight is available. Nevertheless the channel 3 of AVHRR is available at night for all three AVHRR series. For some of the AVHRR instruments the channel 3 is permanently centered at 3.7 µm while for others (e.g. AVHRR/3 on the Metop satellite) the channel 3 mode is switched between 1.6 µm at day and 3.7 µm at night. Instruments such as SEVIRI, AATSR or VIIRS operate as well 1.6 as 3.7 respective 3.9 µm channels permanently, so for these instruments the 3.7 respective 3.9 µm brightness temperature is used as additional input at night. Following Kriebel et al. (2003) the brightness temperature differences between channel 4 and channel 3 and between channel 3 and channel 5 are exploited during night (T43 respective T35). The lower and upper boundaries ($\mathrm{BTD_{min}}$ respective $\mathrm{BTD_{max}}$ in Eq. 9) of the probability estimation interval are 0.5 and 1.5 K in the first and 3 and 5 K in the latter (1 K respective 2 K confidence interval around the thresholds used in Kriebel et al., 2003).

Discussion Paper | Discussion Paper | Discussion Paper | Discussion Paper |

AMTD
8, 4413–4449, 2015

APOLLO_NG – a probabilistic interpretation of the APOLLO legacy

L. Klüser et al.

3 Snow discrimination

The a posteriori snow detection (i.e. detection of falsely identified clouds in the case of snow cover) follows the same approach as the cloud detection scheme. That is, the binary thresholds in Kriebel et al. (2003), originating from Gesell (1989), are expanded by the methodology explained above in order to yield a snow contamination probability. The snow discrimination is only applied over land and for observations with $258\,\mathrm{K} \le T_5 \le 278\,\mathrm{K}$. Also $\Theta_s < 85°$, PT45 = 0 and $P_{DVT} > 0$ are necessary prerequisites for successful snow detection (that means, the pixel must be sunlit, must not be cirrus contaminated and the dynamic visible reflectance test must indicate cloud). Then the snow detection is performed applying Eq. (7) to the channel 3 reflectance R_3 with the thresholds $R_{bg} = 0.1$ and $R_{max} = 0.03$ (which only becomes positive when $R_3 < R_{bg}$) in the case of channel 3 being centered at 3.7 µm. Otherwise, i.e. channel 3 center wavelength of 1.6 µm, $R_{bg} = 0.15$ and $R_{max} = 0.06$. The snow probability is updated once again by using the reflectance ratio between channels 1 and 3 with the confidence interval boundaries $R_{bg} = 20$, $R_{max} = 15$ for the 3.7 µm channel respective $R_{bg} = 6.67$, $R_{max} = 5$ for the 1.6 µm channel.

4 Cloud property retrieval

4.1 Optical depth and effective radius

The mathematics of cloud property retrieval in the original APOLLO follow the approach outlined in Stephens (1978). The general approach and the mathematical treatment have widely been conserved, but a couple of improvements and innovations have gone into the realization of the cloud properties retrieval. Moreover also for cloud properties a probabilistic treatment has been implemented in APOLLO_NG. While in Stephens (1978) absorption was used only for angular correction of the red channel reflectance, now the contrast between one non-absorbing and one absorbing channel ("absorb-

AMTD
8, 4413–4449, 2015

ing” here means that cloud droplets absorb at the respective wavelengths) is used for inferring optical depth and effective radius (Stephens, 1984; Nakajima and King, 1990).

As inherited from the original APOLLO it is assumed that the solution of the radiative transfer problem used in traditional schemes does a reasonably good job for AVHRR. In fact the signal-to-noise ratio as well as the broad spectral response functions of the solar bands of AVHRR (together with the calibration) suggest that using a two stream approximation including above-cloud water vapour absorption in the case of an 3.7 µm NIR channel will provide reasonably good results. In APOLLO_NG the two stream solution of the radiative transfer problem as described in Coakley and Chylek (1975) is used for the non-absorbing and the absorbing channel. This scheme is identical to the scheme used for the original APOLLO cloud property retrieval (Kriebel et al., 1989) and thus truly complies with the APOLLO legacy.

The two stream approach used in APOLLO_NG offers the potential to calculate reflectance online at reasonable high performance. This gives the strong advantage that the method becomes independent of sensor-specific radiance lookup tables and tuning factors (as long as the channel specific cloud single scattering albedo and asymmetry parameter are provided, both essential inputs to the two stream approximation). The second big advantage is that the calculations can be performed for a range of optical depths and effective radii, so that the probabilistic potential can be fully exploited.

Figure 3 exemplarily shows the simulated reflectance in the absorbing and non-absorbing channels of AVHRR for a solar zenith angle of 10° and different pairs of effective radius and optical depth. The red curves connect calculation results with constant effective radius. The black curves indicate constant optical depth, which is mostly related to the reflectance of the non-absorbing channel (Stephens et al., 1984; Nakajima and King, 1990). Orthogonality in the red and black curves would correspond to the possibility of retrieving optical depth and effective radius independently, as is more or less the case for very high optical depths. At lower optical depth the sensitivity to effective radius changes decreases and as a result the uncertainty in retrieved effective radius will become much higher.

AMTD
8, 4413–4449, 2015

For the 3.7 µm channel of AVHRR under daylight conditions it is essential to correct for the thermal emission in order to calculate the reflected part of the signal. Figure 3 clearly shows that getting an improper reflectance in the absorbing channel will cause large uncertainties in the retrieved effective radius, but also in the optical depth. The method of Kaufman and Nakajima (1993) also takes into account above-cloud water vapour absorption for calculation of 3.7 µm reflectance and is applied within APOLLO_NG.

The simultaneous retrieval of cloud optical depth and effective radius (Nakajima and King, 1990) is performed consecutively for each observation for potential liquid water and ice phase clouds. The approach is to calculate optical depths with the respective equations of Coakley and Cox (1975) respective Stephens et al. (1984) from a set of 10 different reflectance values $R_{1,\text{sim}}$ in the red (non-absorbing) channel ranging from 0.05 to 0.95. For each of these 10 values for $R_{1,\text{sim}}$ the distance to the observation R_1 is determined. The weighting factor for each $R_{1,\text{sim}}$ is then calculated assuming a Gaussian distribution around the observation R_1 with a SD of 10 % and the first guess optical depth is then determined by weighting the optical depth values associated with each reflectance value by the thus determined Gaussian weighting factor. Having obtained first guess optical depth the same procedure is repeated for a set of 10 different effective radii and for the reflectance in the absorbing channel, yielding $R_{3,\text{sim}}$. The Gaussian distribution of the thus simulated reflectance around the observation R_3 provides the weighting factors for the effective radius and the resulting effective radius (evaluated for assumed liquid water and ice clouds separately) is again calculated by weighting the input values with the weighting factors. Moreover the first guess optical depth is once again corrected for the influence of the effective radius on the non-absorbing reflectance (through the phase function and thus the backscattered fraction).

Starting values for the effective radius are 2 µm through 20 µm in 2 µm steps for liquid water clouds and 10 µm through 55 µm in 5 µm steps for ice clouds. Necessary single scattering albedo and asymmetry parameter (see Coakley and Cox, 1975; Stephens

AMTD
8, 4413–4449, 2015

et al., 1984) are determined with Mie calculations for liquid water clouds while for ice clouds the optical properties of Baum et al. (2014) are used.

Within APOLLO_NG not only the mean values for optical depth and effective radius are calculated, but also the SD of the thus obtained probability distributions. This methodology easily allows for estimating the uncertainty of the retrieved quantity. Consequently each retrieval is accompanied by an uncertainty estimate, which is a prerequisite e.g. for data assimilation in numerical models.

4.2 Cloud top phase, cloud top temperature and cloud water path

During the previous step two values for cloud optical depth and effective radius have been obtained: one for purely liquid phase clouds and one for ice clouds. Cloud phase discrimination yields the final value for optical depth and effective radius through representative weighting following the probabilistic approach. Therefore the Gaussian distributions for the weighting factors of the simulated channel 3 reflectances (depending on the selected effective radii) are used for evaluating the likelihood of liquid water respective ice clouds. As the absorbing channel is sensitive to the cloud phase as well as to the effective radius, the $R_{3,\mathrm{sim}}$ forward simulations are also very well suited for cloud phase assessment. It is assumed that for both cloud phases not only the minimum distance, but also that the sum over all distance weighting factors should be small, given that the cloud phase well represents the observed cloud. Consequently the first guess of the liquid phase fraction is simply calculated as

$$\mathrm{LPF}_1 = \frac{\sum_j \Phi_j\,(\mathrm{liquid})}{\sum_j \Phi_j\,(\mathrm{liquid}) + \sum_j \Phi_j\,(\mathrm{ice})} \tag{10}$$

where Φ_j denotes the weighting factor for the jth effective radius value for liquid water or ice clouds respectively. If no cirrus cloud is detected, i.e. if the topmost cloud layer is assumed to be opaque, the liquid phase fraction is once more updated with the likelihood of glaciated cloud droplet expressed as a function of temperature. It is assumed

AMTD
8, 4413–4449, 2015

that below the homogeneous freezing temperature of 233.15 K all droplets at cloud top are frozen and that above the pure water freezing point of 273.15 K all cloud droplets are liquid (Pavolonis and Heidinger, 2004). Thus applying Eq. (3) with these boundary thresholds yields an updated liquid phase fraction of

$$\mathrm{LPF} = \frac{\mathrm{LPF}_1 \cdot \left(\frac{T_5 - 233.16\,\mathrm{K}}{40\,\mathrm{K}}\right)}{(1-\mathrm{LPF}_1)\cdot\left(1-\frac{T_5 - 233.16\,\mathrm{K}}{40\,\mathrm{K}}\right) + \mathrm{LPF}_1 \cdot \left(\frac{T_5 - 233.16\,\mathrm{K}}{40\,\mathrm{K}}\right)} \quad (11)$$

for any observation with $233.15\,\mathrm{K} \leq T_5 \leq 273.15\,\mathrm{K}$. Moreover for $T_5 > 273.15\,\mathrm{K}$ LPF = 1 and for $T_5 < 233.15\,\mathrm{K}$ LPF = 0. Cloud optical depth and effective radius are then finally determined by weighting the results for liquid clouds by LPF and those for ice clouds by (1-LPF).

Once cloud optical depth, effective radius and liquid phase fraction are determined, cloud top temperature and cloud water path can be calculated. Cloud top temperature is estimated from channel 5 temperature T_5 and cloud optical depth by inverting the relationship between cloudy and clear radiance (I_{cld} and I_{clr}, respectively) and the channel 5 radiance I_5. The corresponding equation (e.g. Guignard et al., 2012)

$$1 - e^{-\tau} = \frac{I_5 - I_{\mathrm{clr}}}{I_{\mathrm{cld}} - I_{\mathrm{clr}}} \quad (12)$$

then can easily be solved for I_{cld} which then directly yields cloud top temperature through inversion of the temperature–radiance relationship (Planck function in the case of a narrow spectral band, polynomic fit in other cases). I_{clr} is approximated by the background temperature value T_{bg} as determined for the IGT cloud probability. Infrared optical depth τ_{ir} is different from visible optical depth τ_{vis} for non-opaque clouds (e.g. Comstock et al., 2007; Baum et al., 2014). Here the approximation of Chang and Li (2005) is used, which relates τ_{ir} to τ_{vis} by

$$\tau_{\mathrm{ir}} = \frac{\tau_{\mathrm{vis}}}{\mathrm{LPF}\cdot 2.13 + (1-\mathrm{LPF})\cdot 2.56} \quad (13)$$

AMTD

8, 4413–4449, 2015

APOLLO_NG – a probabilistic interpretation of the APOLLO legacy

L. Klüser et al.

Cloud water path can be expressed as a function of optical depth and effective radius as well as extinction efficiency Q_e. For spherical liquid phase cloud droplets $Q_e = 2$, while for ice clouds the extinction efficiency is determined by effective radius (and the crystal shape) and thus is determined from the weighting factors of the effective radius from the optical properties database. Then liquid phase and ice phase extinction efficiencies are weighted according to the liquid phase fraction (the same is done for density ρ) and the cloud water path is calculated as

$$\mathrm{CWP} = \frac{4 \cdot \rho \cdot \tau_{\mathrm{vis}} \cdot r_{\mathrm{eff}}}{3 \cdot Q_e} \tag{14}$$

Besides the liquid phase fraction (or ice phase fraction IPF = 1 − LPF) also cloud top phase is determined to facilitate the interpretation and application of APOLLO_NG results. It is widely controlled by LPF and CTT as well as P_{T45}. Its values and corresponding cloud types are summarised in Table 1.

As a starting point all observations having CTT > 273.15 K or LPF < 0.75 are identified as liquid water clouds. Correspondingly all clouds having CTT ≤ 273.15 K and LPF < 0.05 are initially set to opaque ice clouds. If CTT ≤ 273.15 K and 0.05 ≤ LPF ≤ 0.75 the clouds are classified as supercooled liquid/mixed phase. In the case that P_{T45} indicates thin cloud, presence of cirrus is assumed if $T_5 > 233.15$ (i.e. the cloud is not opaque with cold-top such as deep convective clouds) and CTT < 253.15 K (i.e. the cloud top is reasonably cold for cirrus). Given cirrus has been identified but the optical depth is larger than 2 and more than one test (in that case the T45 test) indicates the presence of clouds (i.e. $H_{\mathrm{inf}} > 0$) it is assumed that more than one cloud layer is present and the overlap flag is set.

In the cloud detection scheme the cloud fraction of each pixel is approximated by the cloud probability as a starting point. Thus observations with $P_{\mathrm{cld}} < 95\,\%$ are assumed to be partially cloudy in the legacy of the original APOLLO. During the cloud property retrieval the first guess cloud fraction is used to estimate the fractional cloud cover within a pixel by averaging the first guess cloud fraction of a surrounding 3 × 3 pixel

AMTD
8, 4413–4449, 2015
APOLLO_NG – a probabilistic interpretation of the APOLLO legacy
L. Klüser et al.

box. It is thus assumed that near cloud edges the information carried by neighbouring pixels translates into subpixel cloudiness (see e.g. Koren et al., 2008; Hirsch et al., 2014 for discussions on the topic of cloud scales).

5 Example results from AVHRR

Figure 4 depicts the RGB composite and cloud mask in the traditional APOLLO quick-look style (Kriebel et al., 2003) for an overpass of NOAA-18 over Europe in HRPT (High Resolution Picture Transmission) projection with 1 km spatial resolution received at the receiving station of the German Aerospace Center (DLR) at Oberpfaffenhofen, South Germany, for 15 July 2008. In the cloud mask image fully cloudy pixels are white, partially cloudy pixels grey, sunglint is yellow, cloud free water is blue and cloud free land brown (see Kriebel et al., 2003). Both images have been produced with APOLLO_NG strictly following the tradition of APOLLO. The cloud mask derived from APOLLO_NG and depicted in Fig. 4 includes all pixels with cloud probability larger than zero.

Figure 5 shows an example of APOLLO_NG cloud probability P_{cld} and the corresponding cloud detection information content H_{inf} for the AVHRR scene on 15 July 2008 in isotropic Mercator projection with 1/30° grid resolution. Clouds have been detected over wide parts of Central and North Europe with high confidence. The information content on the other hand shows, that not in all cases with high cloud probability all cloud tests agree as the variability in H_{inf} is much higher than the variability in P_{cld}. H_{inf} moreover expresses the physical nature of the APOLLO_NG tests, as some (like the spatial coherence or the R21 reflectance ratio test) are useful only under specific cloud conditions. Thus it is not surprising that the information content is highest for cumulus and stratocumulus cloud fields with high spatial variability (e.g. northwest of Great Britain and over Central Europe) and not as high for the cyclonic deep convection in the vicinity of Iceland. In the latter case ice-topped cold clouds with rather high spatial homogeneity prevail, reducing the suitability of the SCT, R21 and T45 tests.

AMTD
8, 4413–4449, 2015

For the retrieval of cloud products a minimum cloud probability of 25 % has been used without any constraint on H_{inf}. Thus the resulting cloud mask is a bit more on the clear conservative side than on the cloud conservative side.

Figure 6 shows the resulting cloud optical depth and effective radius for the same AVHRR scene together with their associated uncertainties. It is evident that the relative uncertainty for cloud optical depth increases with optical depth, especially in cold top (ice) clouds, as can easily be understood from the reduced sensitivity of R_1 to optical depth for high τ_{vis} (Fig. 3) in the case of ice cloud top phase. Moreover high relative uncertainties arise from very low optical depths. Pure ice phase clouds can easily be detected in Fig. 6 by large effective radii (i.e. $R_{eff} > 40\mu m$). While the retrieved effective radius is very sensitive to the ice and liquid water fractions derived during the retrieval, Fig. 6 also nicely shows this sensitivity by the presence of effective radii between 20 and 30 µm. Also for cloud top effective radius the highest uncertainties are observed for high effective radii, i.e. for ice clouds, or in cases of low cloud optical depth.

6 Discussion

The examples presented above showcase the possibility of using the original APOLLO cloud detection metrics and physical parameterizations in a probabilistic manner to increase the information gained from AVHRR observations (or any other satellite observations providing the typical AVHRR heritage channels). With the probabilistic approach the desired degree of conservativeness in the cloud detection can be tuned from clear confident to cloud confident by selecting an appropriate minimum cloud probability for identifying cloud contaminated pixels. In applications of cloud property remote sensing the minimum probability will be set rather high while in cloud masking applications for clear sky remote sensing purposes such as for example aerosol retrieval the minimum probability will be selected rater low. Each evaluation of the cloud mask must thus take into account the purpose of the products as well as the selection of minimum probability. In Fig. 4 it has been shown that cloud probability alone will

AMTD
8, 4413–4449, 2015

result in a valuable cloud mask, but the quality of the cloud detection can furthermore been assessed by the interpretation of the Shannon information content H_{inf} provided along with P_{cld}. The more cloud tests detect potential cloud contamination and thus the higher H_{inf}, the more confidence one can have in the retrieved cloud probability (even if it is a low probability).

Using the Stephens et al. (1984) extension of the original cloud property parameterization scheme allows one to simultaneously retrieving cloud effective radius alongside with optical depth from a two-channel approach like the often-used method of Nakajima and King (1990). This is a major update compared to the original APOLLO scheme, where cloud effective radius was assumed to be constant at 10 µm (e.g. Klüser and Holzer-Popp, 2010). Also the physical cloud products are determined in a probabilistic approach using the distances of online simulations to the observations as a first guess for the probability distribution of cloud properties. In order to be able to perform the simulations online, the two stream approximation already implemented in the original APOLLO is also used in APOLLO_NG, extended by the formulation of the two stream equations for absorbing channels (Coakley and Cox, 1975). We are fully aware that using a two stream approximation will reduce the precision of the reflectance simulations. Nevertheless the advantage of performing the simulations online and thus not being dependent on storing large lookup tables for any angle combination clearly outweighs the loss of precision for the purpose of APOLLO_NG. Moreover, simulating the 3.7 µm reflectance would require very good knowledge about the cloud top temperature a priori. This knowledge typically is not available. Consequently the uncertainties brought about by the estimation of the thermally emitted part of the 3.7 µm band radiance would again result in large errors which would remove all advantages from the precise radiative transfer modelling. This would not be a large problem for sensors such as SEVIRI or VIIRS which also have absorbing channels at 1.6 or 2.2 µm, but for the AVHRR with the 3.7 µm channel the uncertainties introduced by the use of the two stream approximation are expected to not being larger than those of the other estimations and assumptions. Also, given the rather broad channel response functions

AMTD
8, 4413–4449, 2015

of the AVHRR instruments, the uncertainties of the two stream approximation might be acceptable compared to their influence for instruments with finer resolution, where specific features such as water vapour or ozone absorption bands become much more prominent in the radiance observations as they do not “average out” in the integral over the broad spectral response function.

Online simulations together with the probabilistic approach of retrieving cloud properties have the great advantage that uncertainty assessment is an intrinsic by-product of each retrieved variable. Consequently the uncertainty of each observation (i.e. pixel) is estimated from the observations itself. Figure 6 clearly shows the value of such method. Depending on the purpose of the use of APOLLO_NG results these uncertainties also can be used to confine the applications to observations with high confidence only. This will be especially useful in the application of APOLLO_NG in high resolution case studies (e.g. Klüser et al., 2008) or in the field of aerosol-cloud-interaction research (Klüser et al., 2008; Klüser and Holzer-Popp, 2010).

In this study the methodology of the probabilistic APOLLO_NG scheme has been outlined and the specific approaches have been motivated from well-known physical principles and standard methodologies of cloud remote sensing. Cloud detection and cloud property evaluation is currently performed for APOLLO_NG by different means and for a range of sensors. Cloud detection will first be cross compared with cloud detection results of the original APOLLO scheme, which has already been evaluated with SYNOP data for AVHRR and for Europe (Kriebel et al., 2003; Meerkötter et al., 2004). This cross-comparison will be performed for AVHRR, AATSR and SEVIRI. Moreover APOLLO_NG will be run with MODIS (MODerate resolution Imaging Spectroradiometer) and VIIRS observations and will be compared with cloud mask results from the MODIS/VIIRS cloud detection. In order to evaluate the cloud property retrievals, the APOLLO_NG results will also be compared to results of the MODIS/VIIRS cloud retrievals. Using external data as a reference also allows performing sensitivity studies, especially in terms of relationships between minimum cloud probability and false alarm rate respective cloud detection rate. Moreover the availability of a wide range of

AMTD
8, 4413–4449, 2015

APOLLO_NG – a probabilistic interpretation of the APOLLO legacy

L. Klüser et al.

channels including such centered at 1.4, 1.6, 2.3 and 3.7 µm provides the possibility to assess the sensitivity of the retrieved cloud properties to the selection of the absorbing channels and thus to estimate the external uncertainties and potential biases for sensors having only one of the useful channels (like AVHRR).

7 Summary and outlook

The well-known cloud retrieval scheme APOLLO has been revised and a couple of major updates have been implemented. By building on the classical principles for cloud detection and cloud property retrieval, these have been interpreted in a probabilistic way in the APOLLO_NextGeneration cloud retrieval scheme. This study explained the physical and mathematical principles and approaches used in the formulation of the APOLLO_NG scheme and shows example results with AVHRR. One of the major achievements of the APOLLO_NG scheme is to harmonise the legacy of the APOLLO method for all satellite sensors maintaining the so-called AVHRR heritage channels. So far each sensor had its own APOLLO adaptation (see Kriebel et al., 2003; Holzer-Popp et al., 2008; Klüser and Holzer-Popp, 2010), i.e. a harmonization effort was strongly required for future applications and extended evaluation of cloud products and derived information. As the APOLLO_NG makes use of a probabilistic approach to cloud detection, it thus addresses the need of variable cloud detection conservativeness in a broad range of applications (e.g. Holzer-Popp et al., 2013). Traceability of the origins of the reported cloud probability as well as flexible cloud detection thresholds together with a propagation of information allows for a strongly improved characterization of the observed conditions compared to prior versions of APOLLO. New additional interpretations of the cloud detection results such as the Shannon information content of the probabilistic cloud detection moreover feed into the potential to define cloud masks which truly address the purpose of the application. Introducing the retrieval of cloud droplet (and ice crystal) effective radius into the scheme makes APOLLO_NG also a suitable candidate e.g. for aerosol-cloud-interactions research (see Klüser and

AMTD
8, 4413–4449, 2015

Holzer-Popp, 2010) as well as climate studies taking into account droplet size (as well as cloud top phase, which is derived alongside).

APOLLO_NG facilitates the possibility to continue and expand the use of APOLLO in a wide range of applications (e.g. Gesell, 1989; Meerkötter et al., 2004; Holzer-Popp et al., 2008; Klüser and Holzer-Popp, 2010; Schroedter-Homscheidt, 2013). All these applications require a well understood quality (in the meaning of uncertainty and accuracy) as well as clearly documented sensitivities of the APOLLO_NG cloud products. Consequently a subsequent APOLLO_NG evaluation study will use MODIS and VIIRS data to derive the sensitivity to absorbing channel selection between 1.3 and 3.7 µm as well as to cross-compare the cloud property results with the MODIS/VIIRS cloud products at given sensor resolution and geometry.

The article processing charges for this open-access publication were covered by a Research Centre of the Helmholtz Association.

References

Baum, B. A., Yang, P., Heymsfield, A. J., Bansemer, A., Cole, B. H., Merrelli, A., Schmitt, C., and Wang, C.: Ice cloud single-scattering property models with the full phase matrix at wavelengths from 0.2 to 100 µm, J. Quant. Spectrosc. Ra., 146, 123–139, doi:10.1016/j.jqsrt.2014.02.029, 2014.

Chang, F.-L. and Li, Z.: A new method for detection of cirrus overlapping water clouds and determination of their optical properties, J. Atmos. Sci., 62, 3993–4009, 2005.

Coakley, J. A. and Chylek, P.: The two-stream approximation in radiative transfer: including the angle of incident radiation, J. Atmos. Sci., 32, 409–418, 1975.

Comstock, J. M., d'Entremont, R., DeSlover, D., Mace, G. G., Matrosov, S. Y., McFarlane, S. A., Minnis, P., Mitchell, D., Sassen, K., Shupe, M. D., Turner, D. D., and Wang, Z.: An intercomparison of microphysical retrieval algorithms for upper-tropospheric ice clouds, B. Am. Meteorol. Soc., 88, 191–204, 2007.

AMTD
8, 4413–4449, 2015

Frey, R. A., Ackerman, S. A., Liu, Y., Strabala, K. I., Zhang, H., Key, J. R., and Wang, X.: Cloud detection with MODIS. Part I: Improvements in the MODIS cloud mask for collection 5, J. Atmos. Ocean. Tech., 25, 1057–1072, doi:10.1175/2008JTECHA1052.1, 2008.

Gesell, G.: An algorithm for snow and ice detection using AVHRR data an extension to the APOLLO software package, Int. J. Remote Sens., 10, 897–905, 1989.

Guignard, A., Stubenrauch, C. J., Baran, A. J., and Armante, R.: Bulk microphysical properties of semi-transparent cirrus from AIRS: a six year global climatology and statistical analysis in synergy with geometrical profiling data from CloudSat-CALIPSO, Atmos. Chem. Phys., 12, 503–525, doi:10.5194/acp-12-503-2012, 2012.

Hirsch, E., Koren, I., Levin, Z., Altaratz, O., and Agassi, E.: On transition-zone water clouds, Atmos. Chem. Phys., 14, 9001–9012, doi:10.5194/acp-14-9001-2014, 2014.

Holzer-Popp, T., Schroedter, M., and Gesell, G.: Retrieving aerosol optical depth and type in the boundary layer over land and ocean from simultaneous GOME spectrometer and ATSR-2 radiometer measurements, 1, Method description, J. Geophys. Res. Atmos., 107, 2156–2202, doi:10.1029/2001JD002013, 2002.

Holzer-Popp, T., Schroedter-Homscheidt, M., Breitkreuz, H., Martynenko, D., and Klüser, L.: Improvements of synergetic aerosol retrieval for ENVISAT, Atmos. Chem. Phys., 8, 7651–7672, doi:10.5194/acp-8-7651-2008, 2008.

Holzer-Popp, T., de Leeuw, G., Griesfeller, J., Martynenko, D., Klüser, L., Bevan, S., Davies, W., Ducos, F., Deuzé, J. L., Graigner, R. G., Heckel, A., von Hoyningen-Hüne, W., Kolmonen, P., Litvinov, P., North, P., Poulsen, C. A., Ramon, D., Siddans, R., Sogacheva, L., Tanre, D., Thomas, G. E., Vountas, M., Descloitres, J., Griesfeller, J., Kinne, S., Schulz, M., and Pinnock, S.: Aerosol retrieval experiments in the ESA Aerosol_cci project, Atmos. Meas. Tech., 6, 1919–1957, doi:10.5194/amt-6-1919-2013, 2013.

Kaufman, Y. J. and Nakajima, T.: Effect of Amazon smoke on cloud microphysics and albedo – analysis from satellite imagery, J. Appl. Meteorol., 32, 729–744, 1993.

Klüser, L. and Holzer-Popp, T.: Relationships between mineral dust and cloud properties in the West African Sahel, Atmos. Chem. Phys., 10, 6901–6915, doi:10.5194/acp-10-6901-2010, 2010.

Klüser, L. and Schepanski, K.: Remote sensing of mineral dust over land with MSG infrared channels: a new Bitemporal Mineral Dust Index, Remote Sens. Environ., 113, 1853–1867, doi:10.1016/j.rse.2009.04.012, 2009.

Klüser, L., Rosenfeld, D., Macke, A., and Holzer-Popp, T.: Observations of shallow convective clouds generated by solar heating of dark smoke plumes, Atmos. Chem. Phys., 8, 2833–2840, doi:10.5194/acp-8-2833-2008, 2008.

Kolmogorov, A. N.: Logical basis for information theory and probability theory, IEEE T. Inform. Theory, 14, 662–664, 1968.

Koren, I., Oreopoulos, L., Feingold, G., Remer, L. A., and Altaratz, O.: How small is a small cloud?, Atmos. Chem. Phys., 8, 3855–3864, doi:10.5194/acp-8-3855-2008, 2008.

Kriebel, K. T., Saunders, R. W., and Gesell, G.: Optical properties of clouds derived from fully cloudy AVHRR pixels, Beitr. Phys. Atmosph., 62, 165–171, 1989.

Kriebel, K. T., Gesell, G., Kästner, M., and Mannstein, H.: The cloud analysis tool APOLLO: improvements and validations, Int. J. Remote Sens., 24, 2389–2408, 2003.

MacKay, D. J. C.: Information Theory, Inference and Learning Algorithms, Cambridge University Press, Cambridge, UK, 2004.

Meerkötter, R., König, C., Bissoli, P., Gesell, G., and Mannstein, H.: A 14-year European Cloud Climatology from NOAA/AVHRR data in comparison to surface observations, Geophys. Res. Lett., 31, L15103, doi:10.1029/2004GL020098, 2004.

Nakajima, T. and King, M. D.: Determination of the optical thickness and effective particle radius of clouds from reflected solar radiation measurements. Part I: Theory, J. Atmos. Sci., 47, 1878–1893, 1990.

Pavolonis, M. J. and Heidinger, A. K.: Daytime cloud overlap detection from AVHRR and VIIRS, J. Appl. Meteorol., 43, 762–778, 2004.

Rosenfeld, D. and Lensky, I. M.: Satellite-based insights into precipitation formation processes in continental and maritime convective clouds, B. Am. Meteorol. Soc., 79, 2457–2476, 1998.

Rodgers, C. D.: Information content and optimization of high spectral resolution remote measurements, Adv. Space Res., 21, 361–367, 1998.

Rodgers, C. D.: Inverse methods for atmospheric sounding, theory and practice, in: Series on Atmospheric, Oceanic and Planetary Physics, vol. 2, World Scientific Publishing, Singapore, 2000.

Saunders, R. W. and Kriebel, K. T.: An improved method for detecting clear sky and cloudy radiances from AVHRR data, Int. J. Remote Sens., 9, 123–150, 1988.

Schroedter-Homscheidt, M., Oumbe, A., Benedetti, A., and Morcrette, J.-J.: Aerosols for concentrating solar electricity production forecasts: requirement quantification and ECMWF/MACC aerosol forecast assessment, B. Am. Meteorol. Soc., 94, 903–914, 2013.

AMTD
8, 4413–4449, 2015

Shannon, C. E. and Weaver, W.: The Mathematical Theory of Communication, University of Illinois Press, 1949.
Shenk, W. E. and Curran, R. J.: The detection of dust storms over land and water with satellite visible and infrared measurements, Mon. Weather Rev., 102, 830–837, 1974.
Stephens, G. L.: Radiation profiles in extended water clouds. II: Parameterization schemes, J. Atmos. Sci., 35, 2123–2132, 1978.
Stephens, G. L., Ackerman, S., and Smith, E. A.: A shortwave parameterization revised to improve cloud absorption, J. Atmos. Sci., 41, 687–690, 1984.
Yang, P., Wei, H., Huang, H.-L., Baum, B. A., Hu, Y. X., Kattawar, G. W., Mishchenko, M. I., and Fu, Q.: Scattering and absorption property database for nonspherical ice particles in the near- through far-infrared spectral region, Appl. Optics, 44, 5512–5523, 2005.
Warren, S. G.: Optical constants of ice from the ultraviolet to the microwave, Appl. Optics, 23, 1206–1225, 1984.

AMTD
8, 4413–4449, 2015

APOLLO_NG – a probabilistic interpretation of the APOLLO legacy

L. Klüser et al.

Table 1. Cloud top phase values and corresponding cloud types.

cloud phase	corresponding cloud type
1	liquid water cloud
2	supercooled liquid water or mixed phase cloud
3	opaque ice cloud
4	thin cirrus
5	overlap/multilayer clouds (includes also thin clouds over snow)

AMTD
8, 4413–4449, 2015

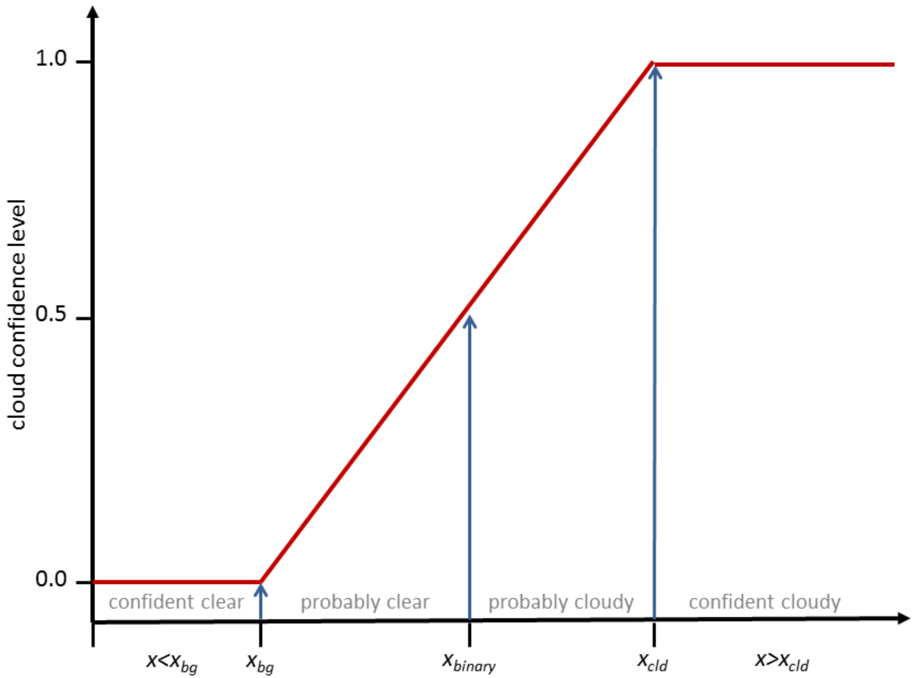

Figure 1. The linear approach of different confidence levels and thresholds used for the cloud probability estimation from an observation of variable x.

AMTD
8, 4413–4449, 2015

APOLLO_NG – a probabilistic interpretation of the APOLLO legacy

L. Klüser et al.

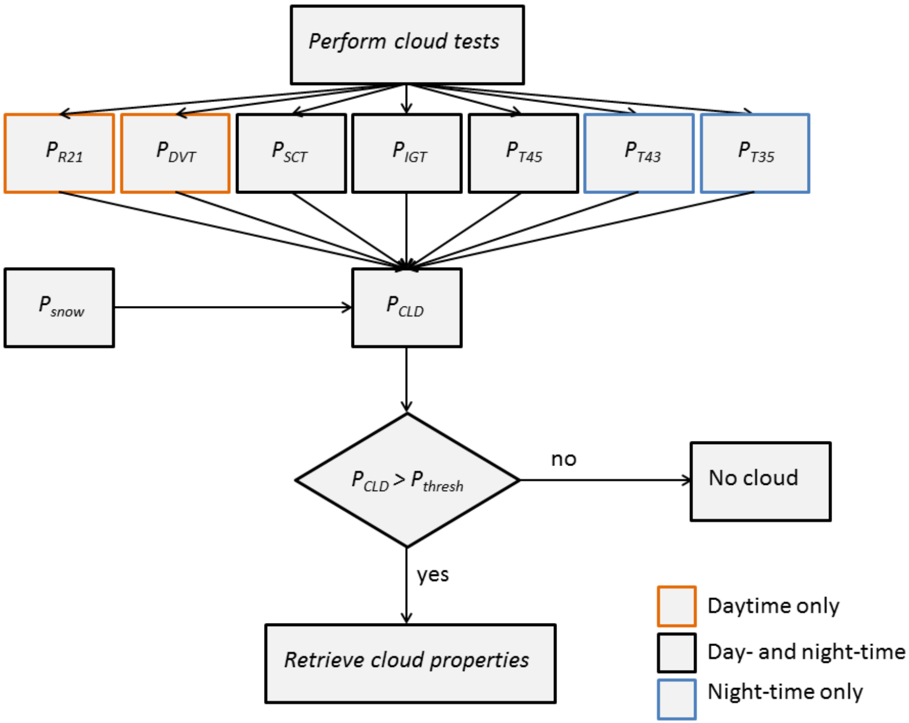

Figure 2. Flowchart of the APOLLO_NG cloud detection and cloud property retrieval scheme.

AMTD
8, 4413–4449, 2015

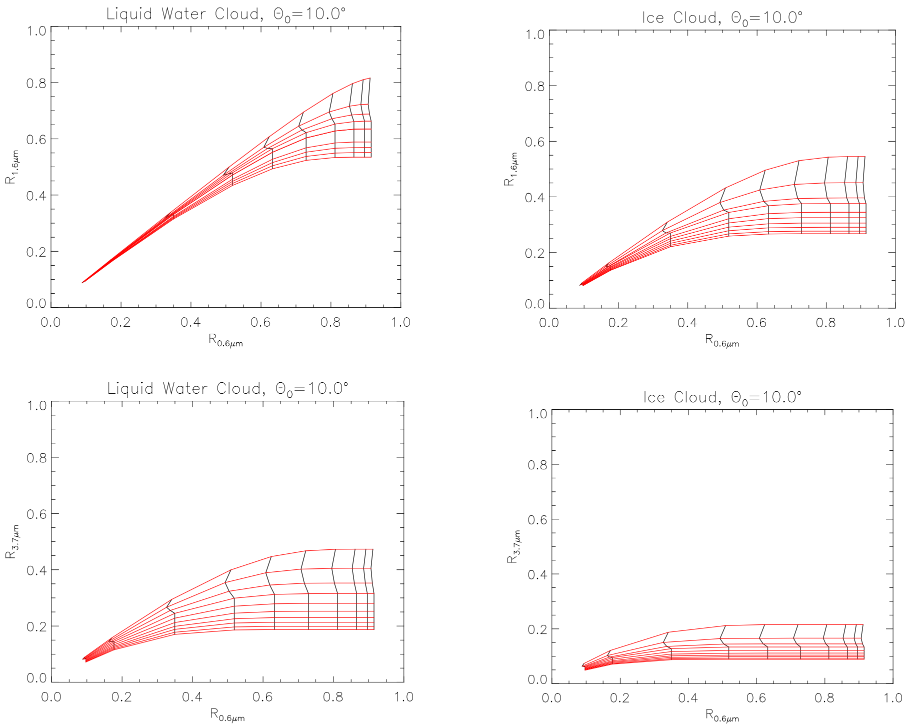

Figure 3. Reflectance of liquid water (left) and ice (right) clouds at the absorbing vs. the nonabsorbing channel for the absorbing channel being centered at 1.6 µm (top) and 3.7 µm (bottom). Cloud reflectance is simulated with the two stream scheme of Coakley and Chylek (1975) for a sun zenith ange or 10° and for various optical depths and effective radii (see text for details).

AMTD
8, 4413–4449, 2015

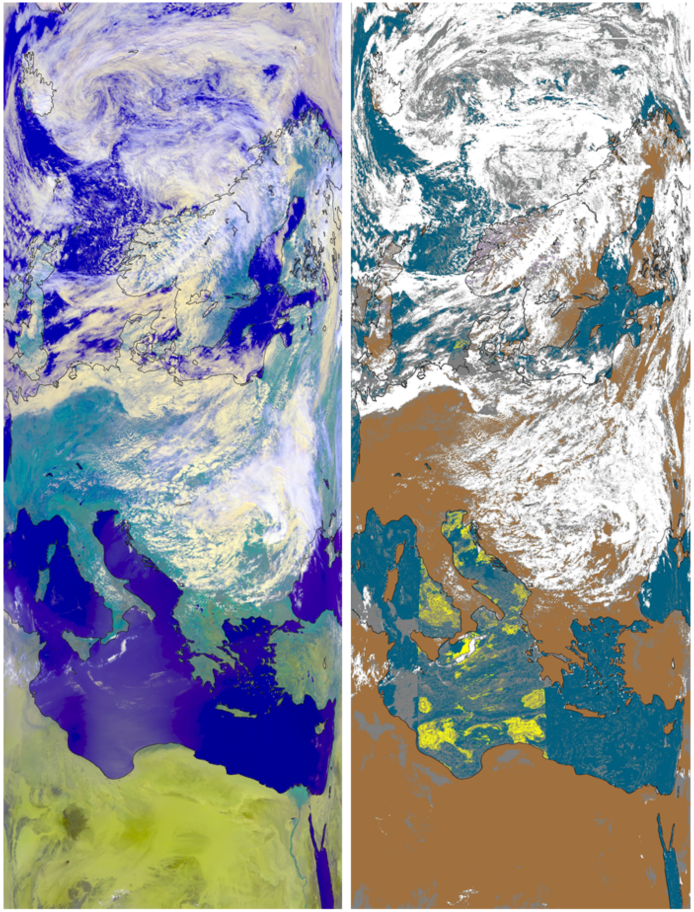

Figure 4. RGB composite and cloud mask in the traditional APOLLO quicklook style (Kriebel et al., 2003; see also text for colour description) from AVHRR on NOAA-18 for 15 July 2008 in orbit projection.

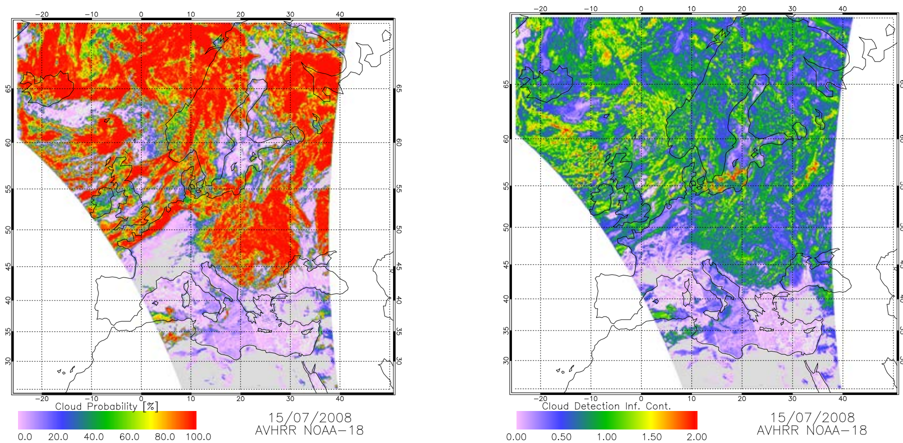

Figure 5. Cloud probability (left) and cloud detection information content (right) from AVHRR on NOAA-18 for 15 July 2008.

AMTD
8, 4413–4449, 2015
APOLLO_NG – a probabilistic interpretation of the APOLLO legacy
L. Klüser et al.

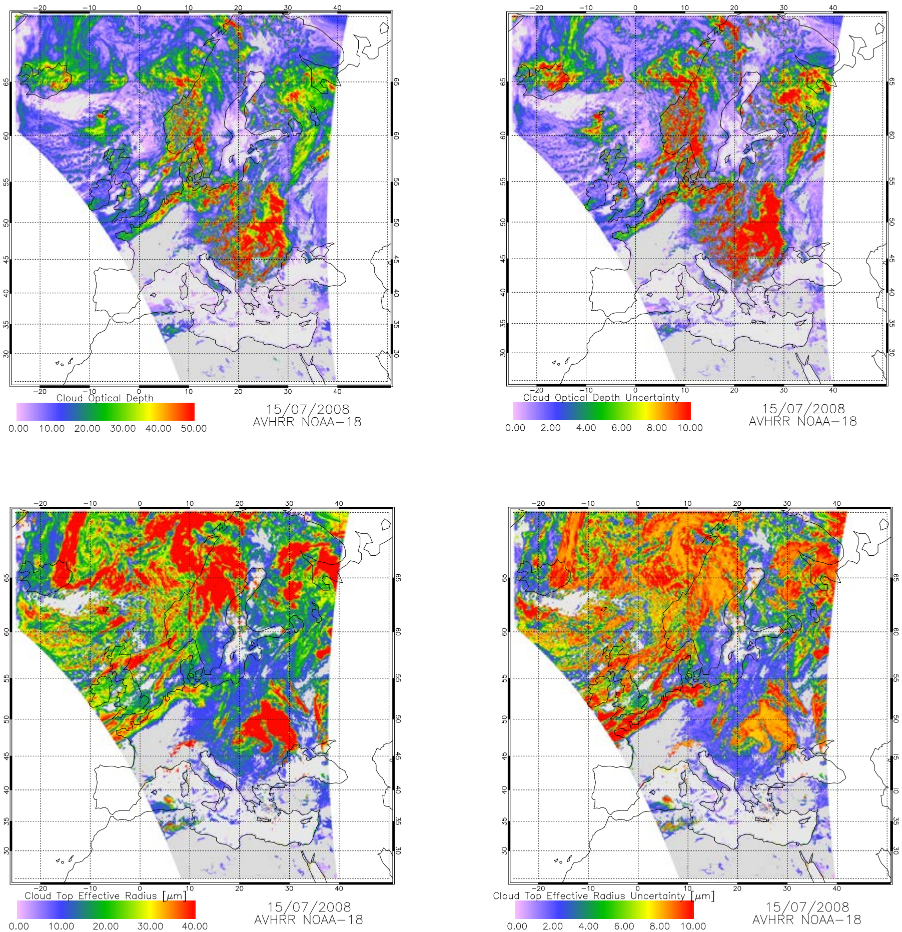

Figure 6. Cloud optical depth (top row) and effective radius (bottom row) retrieval results (left) and associated uncertainties (right) for the same data as in Fig. 4.

AMTD
8, 4413–4449, 2015